Clays Clay Miner., Vol. 71, No. 1:91–105, 2023
https://doi.org/10.1007/s42860-023-00233-9

ORIGINAL PAPER

Enhanced Adsorption Of Humic Acid On Amino-Modified Bentonite

Lei Jiang · Hongjuan Sun · Tongjiang Peng · Juan Du · Lingxi Xia

Accepted: 26 April 2023 / Published online: 25 May 2023
© The Author(s), under exclusive licence to The Clay Minerals Society 2023

Abstract Humic acid (HA) can cause environmental pollution, due to which, its removal from aqueous solutions has become an increasingly important issue. Although bentonite has an affinity for HA, the adsorption capacity of raw bentonite is still poor. As a commonly used organic modifier, 3-aminopropyltriethoxyorganosilane (APTES) exhibits excellent flocculation capability for HA. Therefore, the objective of the present study was to investigate the effectiveness of the addition of 3-aminopropyltriethoxyorganosilane (APTES) to raw bentonite to increase the adsorption of HA from aqueous solution. The experimental results showed that, when the solid-to-liquid ratio was 1:1, the amino-modified bentonite exhibited the highest adsorption capacity (q_{max} = 272.23 mg g^{-1}). The adsorption affinity of amino-modified bentonite was mainly determined by the number of amino groups loaded onto its surface. The adsorption of HA on amino-modified bentonite occurred through electrostatic interactions and hydrogen bonding. These findings demonstrate the excellent potential of amino-modified bentonite in effectively remediating HA pollution.

Keywords Adsorption · Amino-modified bentonite · Electrostatic interactions · Humic acid · Hydrogen bonding

L. Jiang · H. Sun · T. Peng
Key Laboratory of Solid Waste Treatment and Resource Recycle, Southwest University of Science and Technology, Mianyang 621010, China

L. Jiang · H. Sun (✉) · T. Peng
Institute of Mineral Materials and Application, Southwest University of Science and Technology, Mianyang 621010, China
e-mail: sunhongjuan@swust.edu.cn

L. Jiang
School of Life Science and Engineering, Southwest University of Science and Technology, Mianyang 621010, China

J. Du · L. Xia
School of Environment and Resource, Southwest University of Science and Technology, Mianyang 621010, China

Introduction

Humic acid (HA) is a special kind of pollutant. It is a naturally occurring macromolecular organic compound that is found in urban sewage, landfill leachate, and natural water bodies. HA is not toxic, but can give water a yellowish-brown color, and produces an unpleasant taste and odor (Jarvis & Majewski, 2012). More importantly, during the treatment of urban water supplies, HA reacts with chlorine disinfectants to form carcinogenic products, such as chloroform, haloacetic acids, and halo ketones (Li et al., 2017; Tan et al., 2010; Wang et al., 2014). Due to the production of these carcinogenic compounds, HA is considered hazardous to ecosystems and public health.

https://doi.org/10.1007/s42860-023-00233-9 Published online by Cambridge University Press

Nevertheless, when HA and heavy metal ions coexist in water, HA enhances the harmfulness of heavy metals (Wang et al., 2021b; Zhang et al., 2015). This is because HA has large, surface-active functional groups such as -COOH, -OH, -C=O-, -O-CH_3, and -NH_2, which can form complexes with heavy metal ions and promote their migration into the environment. This way, HA affects the occurrence, transformation, bioavailability, and toxicity of heavy metal ions. Therefore, during water treatment, the removal of HA is of particular significance. This also means that developing effective HA-removal technologies is essential. Compared with coagulation and flocculation (Sudoh et al., 2015; Zhou et al., 2018), advanced oxidation techniques (Yang et al., 2021), microbial treatment (Collado et al., 2018), membrane filtration (Lowe & Hossain, 2008), and ion exchange (Bolto et al., 2004), adsorption (Saldaña-Robles et al., 2017; Wang et al., 2021a) is considered to be one of the simplest, most common, most efficient, and most cost-effective techniques (Wang et al., 2022). Humic acid in aqueous solutions can be removed through adsorption or by anchoring it on or to the adsorbent. As a result, it can exert its excellent metal-ion complexing/chelating properties and simultaneously remove the metals from the solution. Controlling the migration of these metal ions in water overcomes the challenge of enhanced mobility of heavy metals after complexation by HA.

Natural surfaces of clay minerals in bentonite have a high affinity for various active functional groups contained in HA. This characteristic, combined with being an inexpensive and abundant resource, has made bentonite particularly interesting to many researchers (Anirudhan et al., 2008; Chen et al., 2017; Doulia et al., 2009; Majzik & Tombacz, 2007; Peng et al., 2005; Salman et al., 2007; Shaker et al., 2012).

Bentonite is a clayey material that is mainly composed of montmorillonite. It is widely used as an adsorbent for heavy metals due to its good adsorption performance and low cost. It has the advantages of being inexpensive and effective as an adsorbent. Bentonite has a large specific surface area (Naderi et al., 2018) as well as a special layered structure (Hua, 2018), excellent ion exchange capacity (Mo et al., 2018), high bonding strength (Ge et al., 2018), and mechanical and thermal stabilities (Bhattacharyya & Ray, 2015; Glatstein & Francisca, 2015). It is a multifunctional material used in many fields and, therefore, is often called the 'multi-purpose clay.' It is widely used to adsorb inorganic or organic pollutants such as heavy metal ions, dyes, and HA. Due to its negative surface charge, natural bentonite is often used to adsorb cationic pollutants (such as Pb^{2+}, Cd^{2+}, Cu^{2+}). Its adsorption capacity for anionic pollutants (such as HA and CrO_4^{2-}) is usually low. In order to improve its adsorption capacity for anionic pollutants, organic modifiers are widely used to modify its surface charge and lipophilicity. Recent studies have demonstrated that adsorbents with amino groups have good adsorption properties for HA, such as graphitic carbon nitride (Wang et al., 2022; Wang et al., 2021a), amino-modified SBA-15 (Tao et al., 2010), polyacrylonitrile fibers (Deng & Bai, 2003a), and APTES (Zhou et al., 2018). Due to the presence of the -NH_2 group, HA can be adsorbed through electrostatic interaction and hydrogen bonds. The above considerations indicate that bentonite, after amino-modification, has a good potential to be used as an adsorbent for removing HA.

The overarching goal of the present work was to find a green, inexpensive, and efficient method for removing HA from aqueous solutions. More specifically, the study aimed to: (1) characterize the properties of APTES-modified bentonite with various solid-to-liquid ratios, properties such as crystal structure, chemical state, functional group, morphology, and zeta potential; (2) study the adsorption behavior of HA using amino-modified bentonite by analyzing the effects of initial concentration, pH, and time, and evaluating the kinetics, adsorption isotherms, and thermodynamic parameters; and (3) elucidate the adsorption mechanism of HA using amino-modified bentonite.

Materials and Methods

Reagents and Materials

All chemicals (standard analytical grade) were used without further purification. Humic acid (fulvic acid $\geq$ 90%; total acid groups of 9-10 meq g^{-1}), APTES (98%), and absolute ethanol were purchased from Aladdin Chemical Co., Ltd. (Shanghai, China). Raw bentonite samples were collected from Xiazijie (Xinjiang, China) and provided by Xinjiang Nonmetallic Minerals Xiazijie Bentonite Co., Ltd. with a CEC

https://doi.org/10.1007/s42860-023-00233-9 Published online by Cambridge University Press

(cation exchange capacity) of 56.3 mmol 100 g^{-1}. The deionized water used in the experiments was made in the laboratory (>18.25 MΩ cm). A 0.45-micron syringe membrane filter was obtained from Tianjin Jinteng Experimental Equipment Co., Ltd. (Tianjin, China) and was used for filtering humic acid solution after adsorption.

APTES-modified bentonite

The amino-modified bentonite was prepared by grafting APTES to the surface according to the methods described in the literature along with minor modifications. A weighed amount of dry bentonite was dispersed in the mixture of ethanol and ammonia (volumetric ratio of 100:0.1). A known amount of 3-aminopropyltriethoxyorganosilane (APTES, 98%) was added to the mixture, and the mixture was stirred (300 rpm) and heated (80°C) in a condenser flask under reflux for 24 h until a brown product formed. The resulting product was washed three times with ethanol and deionization water, and dried in an oven at 60°C for 24 h. In this work, the bentonite, modified with APTES, was labeled as B-N_x, while the unmodified bentonite was labeled as 'bentonite.' Four different solid-to-liquid ratios (w/v) of B-N_x were prepared. In the naming convention of these samples, the x represents the ratio of solid-to-liquid and had values of 0.25, 0.5, 1, and 2.

Experiments on the adsorption of HA on amino-modified bentonite

A series of adsorption experiments was carried out to evaluate the effects of the degree of modification of amino-modified bentonite, initial concentration of HA, pH, time, and temperature on the adsorption capacity of the synthesized adsorbents. First, 1.000 g of HA was dissolved in 0.1 mol·L^{-1} NaOH solution to give a 1 g·L^{-1} suspension of HA. The pH of the desired solution was sequentially adjusted to 3, 5, 7, 9, and 11 using either a HCl or NaOH solution (0.1 mol·L^{-1}). 20 mg of sorbent, i.e. amino-modified bentonite, and 20 mL of HA solution at various pH and concentrations were mixed in a 100-mL conical flask. The mixture was shaken at 200 rpm at a temperature of 25°C for 24 h to ensure adsorption equilibrium of HA on the sorbent. The solution was filtered through a 0.45 µm filter paper. The UV-Vis spectrum of the humic acid solution (obtained using an Evolution™ 300 UV-Vis spectrophotometer; Thermo Fisher Scientific, Inc., Waltham, Massachusetts, USA) revealed an absorption peak (not shown) at 254 nm with the absorption extending into the visible region as well, thus giving the solution a yellowish-brown color, which is consistent with previous research findings (Wang et al., 2022; Zhou et al., 2018). HA concentrations were calculated from absorbance values using the Beer-Lambert Law and a standard curve over the range of 0 to 400 mg HA/L with $R^2 = 0.9997$. The results reported were the average of three replicates, and taken as the equilibrium concentration after adsorption to the adsorbate. The amount adsorbed (q_t) and the adsorption efficiency (r) were calculated using Equations 1 and 2, respectively.

$$q_t = \frac{(c_0 - c_t) \times v}{m} \tag{1}$$

$$r = \frac{c_0 - c_t}{c_0} \times 100\% \tag{2}$$

where q_t is the amount of HA adsorbed onto the amino-modified bentonite at time t (mg g^{-1}), c_0 is the initial concentration of HA (mg L^{-1}), c_t is the equilibrium HA solution concentration at time t (mg·L^{-1}), v is the solution volume (mL), and m is the amount of amino-modified bentonite (mg).

Adsorption kinetics

The kinetics model can directly reflect the speed of mass transfer during the adsorption process. In order to reveal quantitatively the kinetics of the adsorption of HA on amino-modified bentonite, pseudo-first order kinetics (Equation 3) (Gupta et al., 2001), pseudo-second order kinetics (Equation 4) (Ho & McKay, 1999), and intra-particle diffusion (Equation 5) (Ho & McKay, 1998) models were tested.

$$\ln\left(q_e - q_t\right) = \ln q_e - \frac{k_1}{2.303} t \tag{3}$$

$$\frac{t}{q_t} = \frac{1}{k_2 q_e^2} + \frac{1}{q_e} t \tag{4}$$

$$q_t = k_{int} t^{\frac{1}{2}} + c \tag{5}$$

https://doi.org/10.1007/s42860-023-00233-9 Published online by Cambridge University Press

where q_t and q_e are the amounts of adsorption at time t and at equilibrium (mg g^{-1}), respectively; k_1 is the pseudo-first order kinetics adsorption rate constant (min^{-1}); k_2 is the pseudo-second order kinetics adsorption rate constant (g (mg $min)^{-1}$); k_{int} is the intra-particle diffusion rate constant (mg (g $min^{1/2})^{-1}$); and c is the intercept.

Adsorption isotherm models

In order to optimize the design of the entire adsorption system, the most appropriate correlations must be established for the equilibrium conditions. Due to the various adsorption mechanisms, the models used to fit the experimental data were also varied. Among them, the most common ones are the well known Langmuir model (Equations 6 and 7) and the Freundlich model (Equation 8) (Freundlich, 1907; Langmuir, 1916; Langmuir, 1918; Sposito, 1979).

$$q_e = \frac{k_l q_{max} c_e}{1 + K_L c_e} \tag{6}$$

$$R_L = \frac{1}{1 + bc_0} \tag{7}$$

$$q_e = K_F c_e^{\frac{1}{n}} \tag{8}$$

where c_e is the equilibrium concentration of HA in the solution (mg L^{-1}), q_e is the amount of HA adsorbed at equilibrium (mg g^{-1}), q_{max} is the theoretical maximum adsorption capacity (mg g^{-1}), K_L is the Langmuir constant (L mg^{-1}) related to the binding strength, K_F is the Freundlich model constant regarding the adsorption capacity, n is the heterogeneity factor, and c_0 is the highest initial metal ion concentration (mg L^{-1}). R_L is either irreversible ($R_L = 0$), favorable ($0 < R_L < 1$), linear ($R_L = 1$), or unfavorable ($R_L > 1$) adsorption.

Adsorption thermodynamics

In order to reveal the effect and influencing mechanism of temperature on the adsorption of HA, various thermodynamic parameters were calculated using Equations 9, 10, and 11.

$$K_d = \frac{q_e}{c_e} \tag{9}$$

$$\ln K_d = \frac{\Delta S}{R} - \frac{\Delta H}{RT} \tag{10}$$

$$\Delta G = \Delta H - T\Delta S \tag{11}$$

where K_d is the partition coefficient of the mineral-water interface (mL g^{-1}), R is the universal gas constant, T is the temperature (K), ΔH is the enthalpy change (kJ mol^{-1}), ΔS is the entropy change (kJ·(mol $K)^{-1}$), and ΔG is the change in Gibbs free energy (kJ mol^{-1}).

Characterization

The adsorbents before and after adsorption were analyzed using various instrumental techniques. The phase composition of the powder samples was examined with CuKα radiation using a Rigaku D/max IIIA X-ray diffractometer (Tokyo, Japan), with a scanning speed of 10°2θ/min over the range of 5–90°2θ and tube current and voltage of 20 mA and 30 kV, respectively. A Perkin-Elmer Fourier-transform infrared spectrophotometer (Fitchburg, Massachusetts, USA) was used to measure the vibrational energies of the chemical bonds of pellitized samples dispersed in KBr. A Zeiss Ultra 55 field emission scanning electron microscope (Oberkochen, German) was used to prepare the samples using the gold-coated film method. The micro-morphological changes in the samples were observed with the following settings: Resolution: 0.8 nm at 15 kV, 1.6 nm at 1 kV, 4 nm at 0.1 kV; magnifications: 12 to 900,000× (SE) and 100 to 900,000× (BSE). The zeta potential of the samples was measured using a Zetasizer Nano Zs90 zeta potential and nanoparticle size analyzer procured from Malvern (Malvern, UK). A Thermo-Fisher Evolution TM 300 UV-visible spectrophotometer (UV-Vis) (Waltham, Massachusetts, USA) was used to detect the change in absorbance of HA solution at 254 nm. X-ray photoelectron spectroscopy (XPS) measurements were obtained using a Thermo ESCALAB Xi+ X-ray photoelectron spectrometer (Thermo Fisher Scientific Co., Ltd., Waltham, Massachusetts, USA) to explore the changes in chemical bonds of the samples.

https://doi.org/10.1007/s42860-023-00233-9 Published online by Cambridge University Press

Results and Discussion

Preparation of Amino-modified Bentonite

The main chemical components of bentonite samples (Table 1) were SiO_2, Al_2O_3, Fe_2O_3, K_2O, and Cl. The samples also contained a small amount of SO_3 and CaO. The samples were weakly alkaline (pH of 8.76). Moreover, the CEC was 56.3 mmol/100 g, indicating that the samples had good adsorption of cations.

The solid-to-liquid ratios (w/v) of APTES-modified bentonite were sequentially varied through values of 1:0.25, 1:0.5, 1:1, and 1:2. The comparison of XRD patterns for bentonite and modified bentonite (Fig. 4, Table 2) gave the basal spacing at 6.1°2θ (14.36 Å) before the modification. The introduction of APTES shifted the peak to lower angles, giving basal spacings of 15.49 Å for B-$N_{0.25}$, 20.73 Å for B-$N_{0.5}$, 21.21 Å for B-N_1, and 21.29 Å for B-N_2. This suggests that APTES was grafted/inserted into the interlayer domains of the constituent montmorillonite (Mnt) of the bentonite (Bertuoli et al., 2014; Huskic et al., 2013). However, with the addition of APTES, the increase in basal spacing was non-linear, suggesting that APTES molecules were first grafted onto the Mnt surface, and then entered the interlayer space. Eventually, further increases in the amount of APTES failed to increase the interlayer spacing, indicating that the adsorption of APTES in the interlayers reached the maximum. The structure of hydrolyzed APTES was similar to an alkyl chain with a height of ~4 Å (He et al., 2005). Therefore, the observed maximum interlayer spacing of 21.29 Å indicated that APTES was arranged in not more than two parallel bilayers between the Mnt layers.

After APTES modification, the contact angle and specific surface area measurements (Table 2) of bentonite revealed that, with the increase in the APTES loading, the contact angle increased due to the presence of more hydrophobic surface. Moreover, the APTES loading affected the specific surface area, which increased from 29.88 $m^2\ g^{-1}$ for the raw bentonite to a maximum of 150.35 $m^2\ g^{-1}$ for B-$N_{0.25}$. The value decreased to 9.22 $m^2\ g^{-1}$ for B-N_1, and increased again to 36.56 $m^2\ g^{-1}$ for B-N_2. When the solid-to-liquid ratio was 1:0.25, a sharp increase in the specific surface area was observed, which was due to the dispersion of Mnt by anhydrous ethanol that was used in the modification process. Only a small amount of APTES reacted with the external Mnt surfaces and did not enter the interlayer. As the amount of APTES increased, it gradually moved into the interlayers, resulting in a gradual reduction in the specific surface area. When the solid-to-liquid ratio was 1:2, some APTES self-polymerized, which could not be accommodated in the interlayers. For this reason, the surface occupied by APTES and the interlayer spacing of Mnt decreased, while the specific surface area increased.

Table 2 Basal spacing (d_{001}), contact angle, and specific surface area of raw and amino-modified bentonite

Sample	d_{001} (Å)	Contact angle (°)	S_{BET} ($m^2 \cdot g^{-1}$)
Bentonite	14.36	10.61	29.88
B-$N_{0.25}$	15.49	30.72	150.35
B-$N_{0.5}$	20.73	34.48	31.56
B-N_1	21.21	34.59	9.22
B-N_2	21.29	33.86	36.56

The mechanism for the grafting of APTES onto bentonite is proposed as follows (Fig. 5). The Si-O groups forming the basal surfaces of Mnt are known to form hydrogen bonds with polar molecules such as H_2O (Yan et al., 1996a; Yan et al., 1996b; Yan et al., 1996c; Yan et al., 1996d; Yan & Stucki, 1999; Yan & Stucki, 2000). Such groups in the hydrolyzed form of APTES become hydrogen bonded to the basal surfaces both internal and external to the interlayer region. This could be considered a condensation reaction (Bertuoli et al., 2014). The irreversible grafting reaction between Mnt and APTES included two basic steps (He et al., 2005). At first, the APTES molecules occupied only the external surfaces and the specific

Table 1 Chemical composition of raw bentonite (wt.%)

Chemical Composition	SiO_2	Al_2O_3	Fe_2O_3	K_2O	Cl	SO_3	CaO	MgO	Na_2O	LOI*
wt.%	66.57	18.37	6.23	1.80	1.74	1.11	0.96	0.94	0.83	0.26

*LOI: Loss on Ignition

https://doi.org/10.1007/s42860-023-00233-9 Published online by Cambridge University Press

surface area remained unchanged. Then, the APTES molecules expanded the interlayers as they moved into them, thus increasing the specific surface area. Previous studies demonstrated that APTES molecules were arranged in parallel bilayers between the natural Mnt layers (He et al., 2005).

Surface-charge Characteristics of Amino-modified Bentonite and Humic Acid

Zeta potential measurements (Fig. 1) revealed that raw bentonite, amino-modified bentonite, and HA were all negatively charged at the pH values of 2, 3, 5, 7, 9, and 11. HA is well known as an anionic polyelectrolyte over a wide pH range. As a mineral, raw bentonite is mainly composed of Mnt, and has a permanent negative charge on its basal surfaces due to isomorphic substitution. The amino-modified bentonite obtained from APTES modification had amino silane cations. With the decrease in pH, the zeta potential of amino-modified bentonite increased distinctly.

Adsorption of HA Using Amino-modified Bentonite

Effects of pH, initial concentration, and degree of modification of amino-modified bentonite on the adsorption of HA

The adsorption of HA onto amino-modified bentonite is significantly affected by pH, HA concentration, and modification degree (Fig. 2a-e). As pH increased gradually from 3 to 11, the adsorption of HA onto amino-modified bentonite with different modification degrees decreased. The effect of HA concentration on adsorption is also related to pH. Under acidic conditions (pH 3 and 5), the adsorption increased with increasing HA concentration (10–400 mg L^{-1}). At HA concentration of 400 mg L^{-1} and pH 3, the adsorption of HA onto amino-modified bentonite with different modification degrees reached a maximum, namely 203.56, 128.21, 133.84, 158.37, and 135.11 mg g^{-1}, respectively. Under neutral or alkaline conditions (pH 7, 9, and 11), the adsorption increased with increasing concentration to a certain optimal point, and then

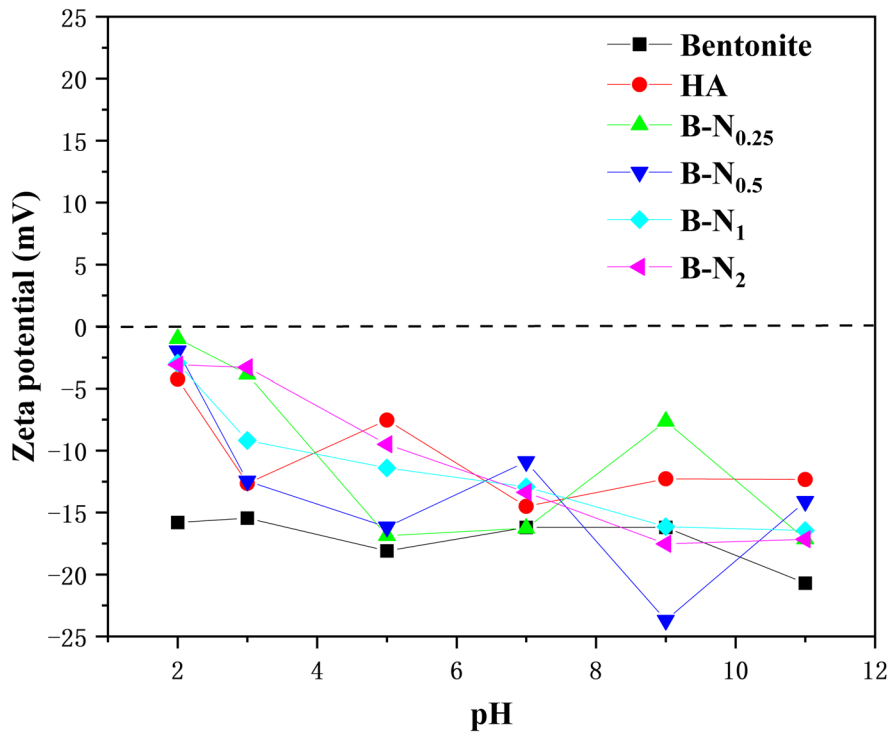

Fig. 1. Zeta potential of bentonite, amino-modified bentonite, and HA at various pH

https://doi.org/10.1007/s42860-023-00233-9 Published online by Cambridge University Press

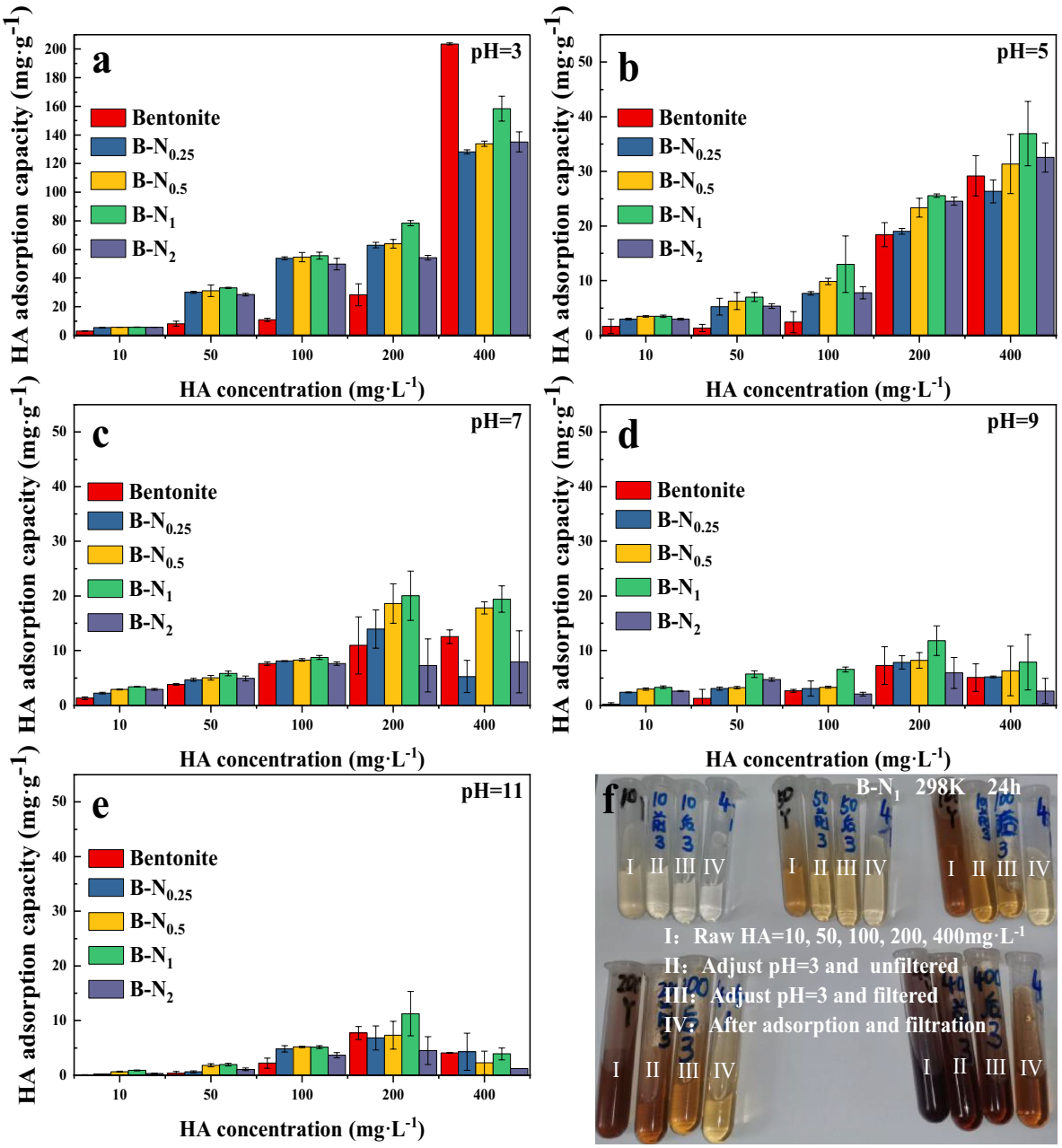

Fig. 2. Adsorption of HA by raw and amino-modified bentonite at various pH (T = 25°C; t = 24 h): **a**–**e** effect of B-N_x as adsorbent on the extent of HA adsorption; **f** visible changes in color of samples from **a**–**e**

decreased. The adsorption also first increased and then decreased with increasing modification degree (V_{APTES}:m_{Mnt} from 0 to 2), with B-N_1 (V_{APTES}:m_{Mnt} = 1) exhibiting the greatest adsorption of HA. Considering the above three factors, when pH was 3 and HA concentration was 400 mg L^{-1}, B-N_1 exhibited the greatest adsorption of HA, which was 158.37 mg g^{-1}. An anomalous phenomenon that does not conform to the above patterns was also observed, where the adsorption of HA onto raw bentonite reached 203.56 mg g^{-1} at pH 3 and HA concentration of 400 mg L^{-1}.

https://doi.org/10.1007/s42860-023-00233-9 Published online by Cambridge University Press

pH is a critical factor that affects the surface chemistry of amino-modified bentonite and the conformation of HA. At low pH, the surface of amino-modified bentonite became positively charged due to protonation of -NH_2, inducing electrostatic adsorption of negatively charged HA (Wang et al., 2022). As the solution pH increased, the deprotonation of the surface of amino-modified bentonite led to a decrease in HA adsorption. This indicated that the adsorption capacity of amino-modified bentonite for HA is related to the surface-loaded -NH_2 groups. In addition, under low pH conditions, the protonated HA became coiled and aggregated, forming droplet aggregates, which favored HA adsorption (Deng & Bai, 2003b). At pH 2.5, the average hydrodynamic diameter of HA aggregates (50 mg L^{-1}) increased gradually from ~460 nm to 1700 nm within 1 h (Lan et al., 2022). As the droplets increased gradually and became spherical, the HA aggregates become more compact. With higher HA concentrations, more large aggregates, precipitation, and even flocculation can occur. At pH 3 and with HA = 400 mg L^{-1}, the addition of raw bentonite promoted the aggregation of HA, resulting in a large number of large HA aggregates (>460 nm) in the system. After filtration through a 0.45 μm membrane, the large HA aggregates were removed, and the supernatant became clear (Fig. 2f). The absorbance also decreased, and the calculated adsorption capacity increased. This is probably the reason for the anomalous adsorption capacity of raw bentonite for HA. As the degree of modification increased, the adsorption capacity of amino-modified bentonite for HA increased gradually to an optimal point and then decreased. This indicated that the number of surface-loaded -NH_2 groups also affected the adsorption capacity of amino-modified bentonite for HA. Therefore, considering the cost and performance of adsorbents, B-N_1 was selected as the most suitable adsorbent for further experiments.

Isothermal adsorption, intraparticle diffusion, and adsorption kinetics and adsorption thermodynamics of HA on amino-modified bentonite

From the adsorption results of HA on amino-modified bentonite at various pH and initial concentrations of HA, sample B-N_1 had the best adsorption performance for HA, so it was selected as the optimal adsorbent to be used in subsequent experiments.

The kinetics data of HA adsorption on B-N_1 fitted the pseudo-second order model well, as indicated by the coefficient of determination (R^2 = 0.921) (Table 3). The results showed that the adsorption of HA was related to the surface groups of B-N_1 (Doulia et al., 2009). The kinetic process (Fig. 3a) showed a sharp increase during the initial phase of adsorption (<120 min), which was attributed to the abundance of available exchange sites, strong chelation, and efficient mass transfer. When the contact time between B-N_1 and HA was prolonged, the HA adsorbed on B-N_1 increased slowly. The large adsorption capacity in the first 2 h was due to the availability of abundant adsorption sites on B-N_1, which were gradually filled with HA molecules over time (Dehghani et al., 2018). When many adsorption sites on the surface of B-N_1 were occupied, the intermolecular repulsion force of the adsorbed HA increased. The rate of adsorption decreased gradually. In order to elucidate the diffusion mechanism, the intraparticle diffusion model was used to simulate the diffusion process of HA (Fig. 3b). The results indicated that the adsorption of HA involved two stages. First, HA was transported to the outer surfaces of B-N_1 through the liquid film, and then migrated from the outer surfaces into the inner pores. Therefore, the diffusion step mainly consists of membrane and intraparticle diffusion (Wang et al., 2022). The Freundlich model gave the best fit of the data for HA adsorption on amino-modified bentonite (Wang et al., 2021a) (R^2 = 0.958-0.973) (Fig. 3c, Table 4). Furthermore, B-$N_{0.25}$ showed a greater adsorption affinity (K_F) than other amino-modified bentonites. The fitting results of the Langmuir model (Table 4) showed the maximum monolayer

Table 3 Kinetic parameters of HA adsorption on amino-modified bentonite

Adsorbent	c_0 (mg·L^{-1})	qk_1 (mg·g^{-1})	Pseudo-first order model			Pseudo-second order model		
			$q_{e,cal}$ (mg·g^{-1})	k_1 min^{-1}	R^2	$q_{e,cal}$ (mg·g^{-1})	k_2 g·(mg·min^{-1})	R^2
B-N_1	100	54.271	45.456	0.010	0.877	51.484	2.506	0.921

https://doi.org/10.1007/s42860-023-00233-9 Published online by Cambridge University Press

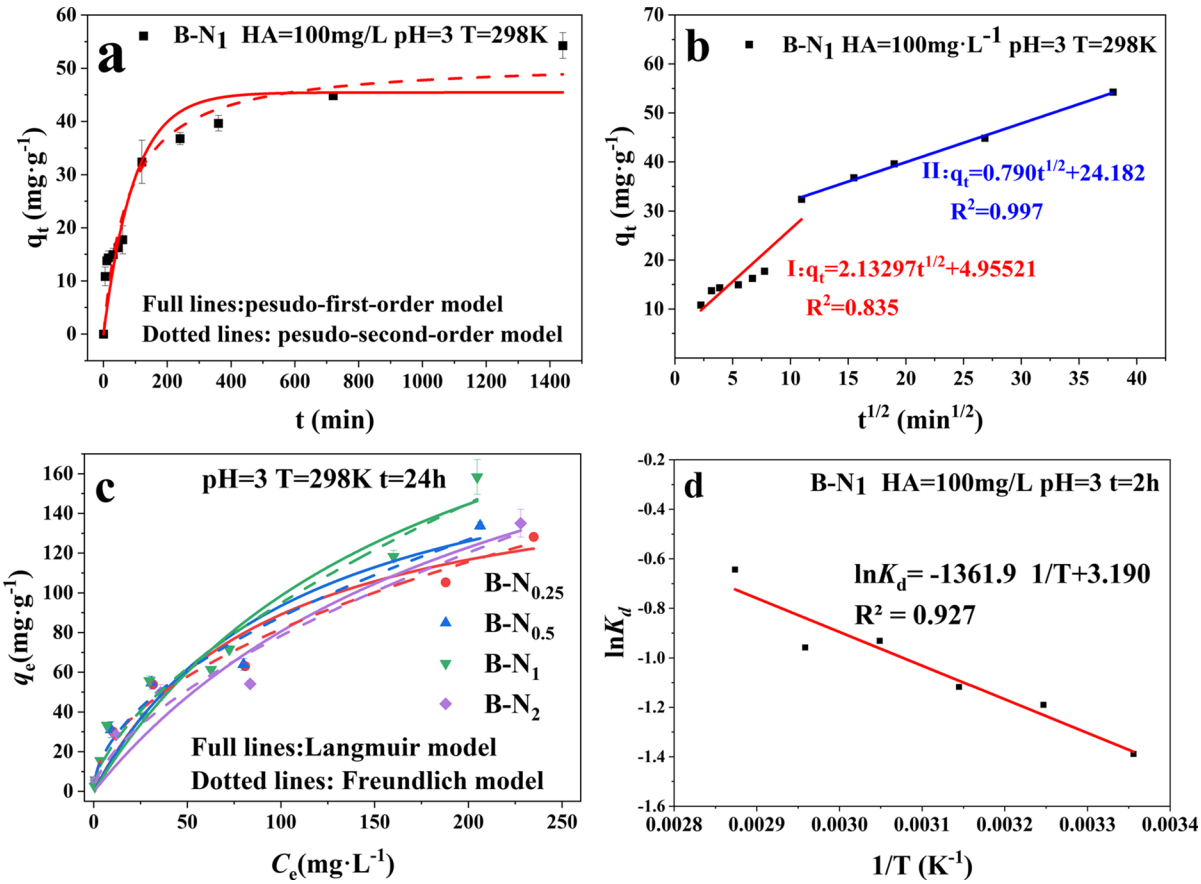

Fig. 3. **a** Adsorption kinetics of HA onto B-N_1; **b** internal diffusion for HA uptake by B-N_1; **c** adsorption equilibrium isotherms of HA onto B-$N_{0.25\text{-}2}$; **d** thermodynamic parameters of adsorption of HA on B-N_1

Table 4 Isothermal adsorption constant and coefficient of determination for the adsorption of HA on amino-modified bentonite

Adsorbent	Langmuir					Freundlich	
	q_m (mg·g^{-1})	b (L mg^{-1})	R_L	R^2	n	K_F (mg·g^{-1})	R^2
B-$N_{0.25}$	169.015	0.011	0.185	0.930	2.004	8.229	0.973
B-$N_{0.5}$	193.505	0.009	0.217	0.915	1.890	7.690	0.965
B-N_1	272.230	0.006	0.294	0.940	1.633	5.659	0.969
B-N_2	258.887	0.004	0.385	0.923	1.620	4.571	0.958

adsorption of HA on B-$N_{0.25}$, B-$N_{0.5}$, B-N_1, and B-N_2 to be (q_m) 169.015, 193.505, 272.230, and 258.887 mg/g, respectively. Of these, the maximum adsorption capacity of B-N_1 was the highest. The respective R_L values were calculated to be 0.185, 0.217, 0.294, and 0.385, indicating a favorable adsorption of HA by amino-modified bentonite (Bagherifam et al., 2021).

In terms of thermodynamic parameters (Table 5), ΔH was positive, indicating that the adsorption of HA by B-N_1 was an endothermic process. On the other hand, ΔG was positive and decreased with the increase in temperature, indicating that high temperature was more conducive to the adsorption of HA. Additionally, B-N_1 was compared with the reported

https://doi.org/10.1007/s42860-023-00233-9 Published online by Cambridge University Press

Table 5 Thermodynamic parameters of adsorption of HA on B-N_1

Adsorbent	ΔH (kJ·mol^{-1})	ΔS (J·mol^{-1})	ΔG (kJ·mol^{-1})					
			298 K	308 K	318 K	328 K	338 K	348 K
B-N_1	11.323	26.524	3.419	3.153	2.888	2.623	2.358	2.092

bentonite-based adsorbents and other samples for adsorption of HA (Table 6). The results showed that B-N_1 was more competitive than other adsorbents in terms of the removal of HA from aqueous solution.

Structure, Morphology, and Spectroscopic Properties of Adsorbed Samples

Comparison of the XRD patterns from the samples before and after HA adsorption (Fig 4a) showed that the d_{001} value increased significantly after modification with the APTES, indicating that it entered the Mnt interlayers and was arranged in parallel double layers. After the adsorption of HA, the basal spacing increased slightly compared with that before the adsorption, suggesting that small HA molecules in HA may have entered the Mnt interlayer during adsorption. Meanwhile, the raw bentonite sample was not purified before the modification. After modification and adsorption, partial loss of Mnt in the sample was observed during the suction filtration process. Enhancement of the quartz peak in the sample was observed as a result.

SEM images showed (Fig. 4b) that the bentonite had a characteristic layered pattern of irregular clay folds. After loading APTES, a smooth and dense structure appeared due to the covering of APTES, proving that APTES successfully modified the bentonite. Comparison of the SEM images of HA and B-N_1-xf-HA confirmed that B-N_1 was wrapped onto the surface of HA.

Most of the characteristic FTIR vibration positions of bentonite remained unchanged after amino modification (Fig. 4c). The characteristic peaks of unmodified bentonite were present at 3698 and 3622 cm^{-1}, which were due to the stretching vibrations of Al-OH. Moreover, the symmetric and asymmetric O-H overlapping stretching vibration of the adsorbed water molecules caused a broad band near 3436 cm^{-1}. The band at 1640 cm^{-1} was the manifestation of the bending vibration of O-H. The asymmetric stretching vibration of the Si-O-Si tetrahedra in Mnt caused the vibration near 1035 cm^{-1}. After APTES modification, the stretching vibration peak of -CH_2 (Mekidiche et al., 2021) was observed at 2937 cm^{-1}. At the same time, many small peaks in the range 1490-1580 cm^{-1} appeared, confirming the presence of the organic modifier in the bentonite. Perhaps the amino groups grafted onto bentonite were involved in the coupling of HA through electrostatic or hydrogen bonding.

Table 6 Comparison of HA adsorption performance of amino-modified bentonite and other samples

Adsorbent	q_m (mg·g^{-1})	pH	T	Ref
CNU-575-3	164.06	3	NA	(Wang et al., 2022)
Ca-Mt	71.962	5	298	(Zhang et al., 2019)
Na-Mt	28.597			
bentonite–chitosan composite	91.4	4	298	(Dehghani et al., 2018)
Montmorillonite	9.0±0.5	4	298	(Chen et al., 2017)
Kaolinite	9.0±0.3			
Am–PAA–B	174.03	2	323	(Anirudhan et al., 2008)
APTES functionalized stereoscopic porous activated carbon	156.00	6	303	(Zhou et al., 2019)
APTES modified palygorskite (PA-NH_2)	71.43	NA	298	(Wang et al., 2017)
B-N_1 (Bent-NH_2)	272.230	3	298	This study

https://doi.org/10.1007/s42860-023-00233-9 Published online by Cambridge University Press

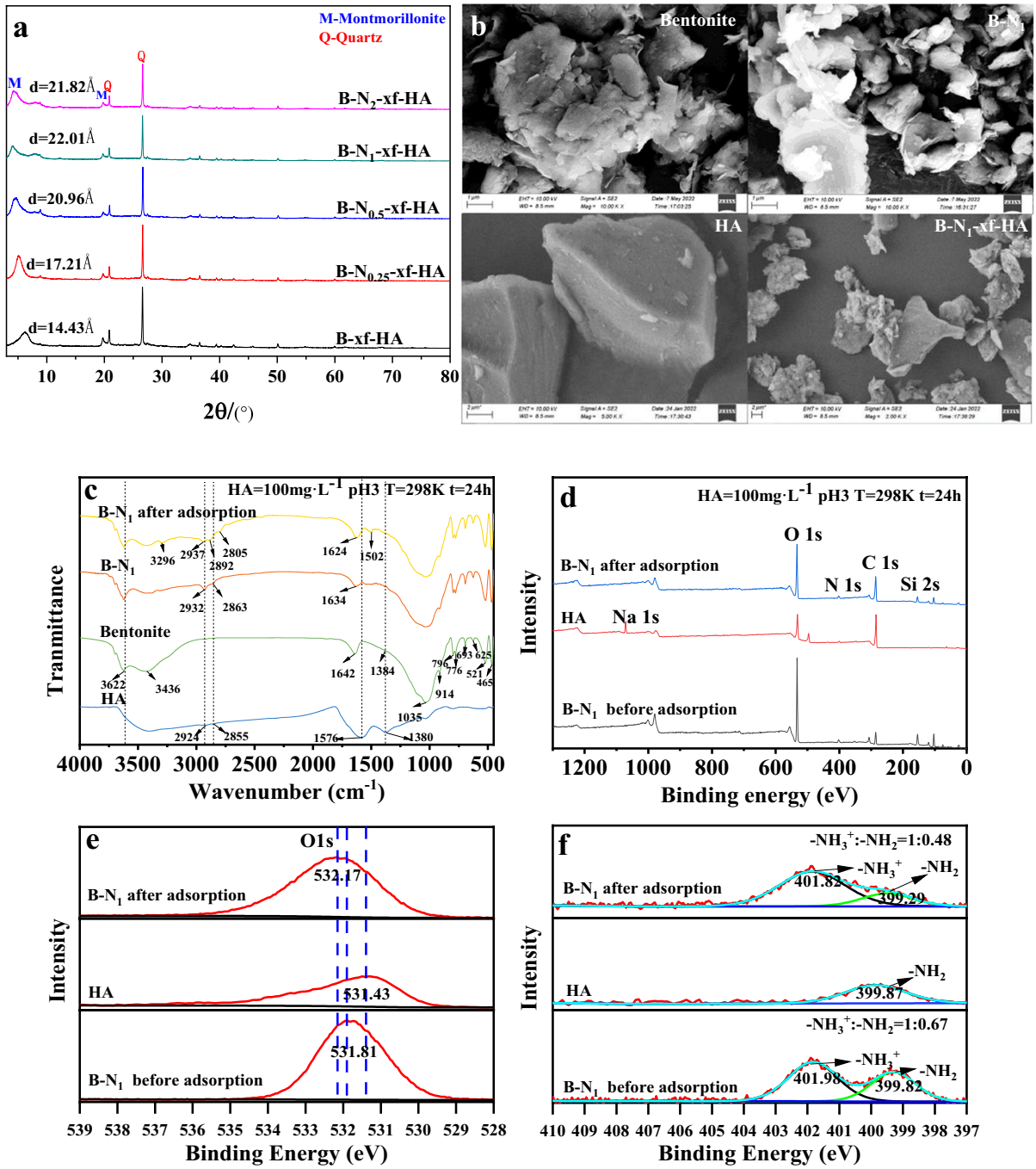

Fig. 4. Comparison of **a** X-ray diffraction, **b** SEM, **c** FTIR, **d** XPS scans, **e** O1s XPS spectra, and **f** N1s XPS spectra before and after adsorption of HA by raw and amino-modified bentonite

In order to clarify the adsorption mechanism of HA by B-N_1, a comparison of XRD, FTIR, and XPS results before and after adsorption was conducted. The characteristic peaks of the full XPS spectra of HA, B-N_1, and B-N_1-xf-HA (Fig. 4d) at 532.17, 401.87, 284.80, and 102.73 eV were attributed to the binding energies of O1s, N1s, C1s, and Si2s, respectively. Compared to O1s peaks before and after the

https://doi.org/10.1007/s42860-023-00233-9 Published online by Cambridge University Press

adsorption (Fig. 4e), the O1s peaks of B-N_1-xf-HA showed apparent shifts to higher binding energies, with transitions of ~0.36 eV. This transition indicates that the oxygen-containing groups of HA were electronically coupled to the -NH_2 groups on the surface of B-N_1 (Wang et al., 2021a). The peaks at 399.29, 399.82, and 399.87 eV were assigned to the nitrogen atom in the -NH_2 group (Fig. 4f), whereas those at 401.82 and 401.98 eV were ascribed to the protonated amine (-NH_3^+). Moreover, the N1s peak shifted to lower binding energy during the adsorption of HA. Combined with the high resolution spectrum of O1s, the electronic coupling between the amino group on the bentonite surface and the oxygen-containing group of HA was proven (Feng et al., 2019). At the same time, the area ratio of -NH_3^+:-NH_2 of B-N_1 was 1:0.67. After the adsorption, the ratio changed to 1:0.48, indicating that protonated amino groups may have been generated on the surface of B-N_1, induced by H-bonds under low pH conditions. Furthermore, lower pH induced more protonated amino groups for the adsorption of HA. This may explain why amino-modified bentonite effectively adsorbs HA under low pH conditions (Deng & Bai, 2004; Quan et al., 2020; Zhao et al., 2008); upon protonation, -NH_2 switches from an electron-donating to an electron-accepting state. One may speculate, therefore, that electrostatic interactions may exist mainly between the protonated -NH_2 and -COO^-. As revealed earlier, the adsorption of HA on amino-modified bentonite is mainly regulated by electrostatic interactions and hydrogen bonds (Xie et al., 2020; Zhang et al., 2021).

Mechanism Analysis

In summary, the preparation process of amino-modified bentonite and its adsorption mechanism for HA (Fig. 5) involved the grafting of APTES into the Mnt interlayers, on their outer surfaces, and at layer edges to obtain amino-modified bentonite. Next, in an aqueous solution at pH 3, HA was adsorbed onto amino-modified bentonite. The -COO^- on the surface of HA became adsorbed to the -NH_3^+ on the surface of B-N_1

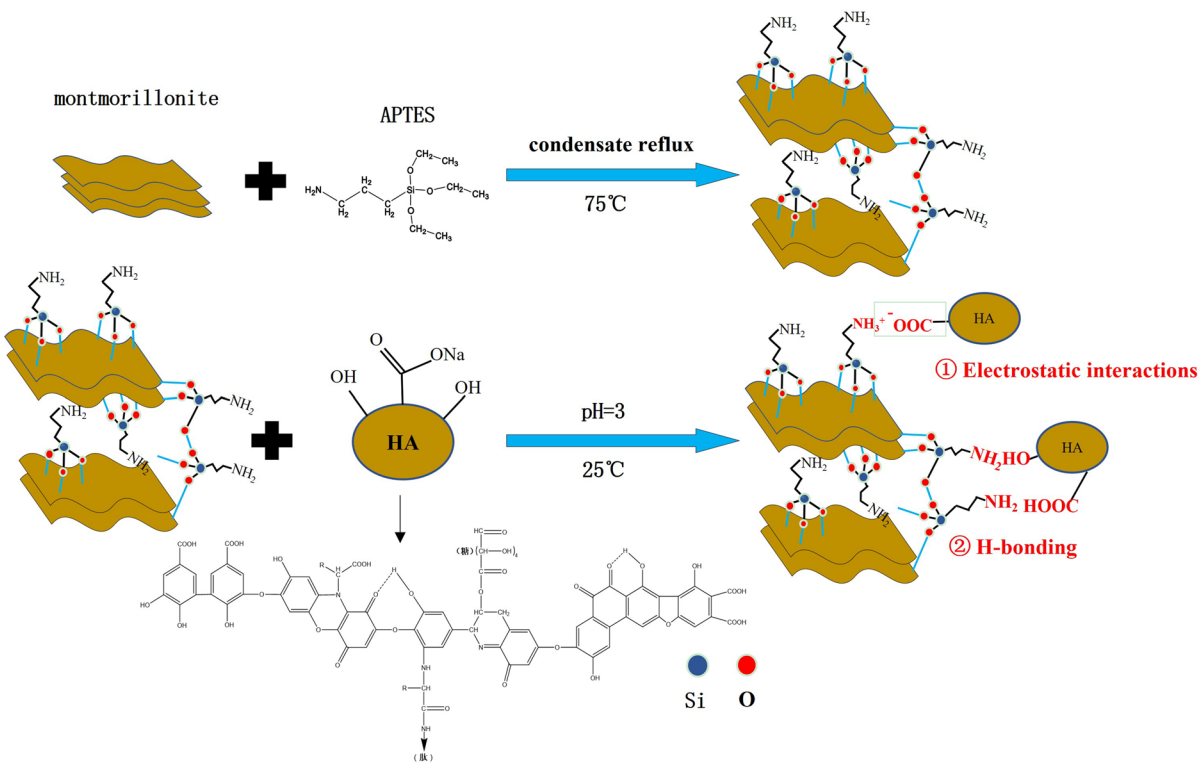

Fig. 5 Schematic diagram of the preparation process of amino-modified bentonite and its adsorption mechanism for HA

https://doi.org/10.1007/s42860-023-00233-9 Published online by Cambridge University Press

through electrostatic interaction, which is the primary adsorption process, and also through the formation of hydrogen bonds between the unprotonated amino groups on the surface of amino-modified bentonite and the oxygen-containing groups of HA. Both of these adsorption mechanisms were strongly affected by the pH. As the pH increased, the amino groups of amino-modified bentonite deprotonated. The electrostatic interactions and hydrogen bonds weakened or became ineffective, which led to the desorption of HA.

Conclusions

In this study, a new type of amino-modified bentonite adsorbent was prepared through APTES modification using raw bentonite. The adsorbent had a high adsorption capacity for HA in an aqueous solution. The results showed that at 298 K, the maximum adsorption capacity of B-N_1 was 272.23 mg g^{-1}. The adsorption kinetics fit the pseudo-second order model, as well as the Freundlich model. The results also showed that the adsorption affinity was mainly related to the number of amino groups loaded on the surface of the bentonite. The adsorption mechanism of HA on amino-modified bentonite consisted of electrostatic interactions and hydrogen bonding. The study showed that amino-modified bentonite has significant potential to be applied as an adsorbent of HA in aquatic bodies.

Acknowledgments This work was supported by the National Key R&D Program (2018YFC1802902).

Declarations

On behalf of all authors, the corresponding author approves all ethical responsibilities for publication in the journal *Clays and Clay Minerals* and consent to participate. This manuscript has not been published in full or in part previously and has not been submitted elsewhere nor is it under consideration by another journal.

Conflict of Interest The authors declare that they have no conflict of interest.

References

Anirudhan, T. S., Suchithra, P. S., & Rijith, S. (2008). Amine-modified polyacrylamide-bentonite composite for the adsorption of humic acid in aqueous solutions. *Colloids and Surfaces A-Physicochemical and Engineering Aspects, 326*, 147–156.

Bagherifam, S., Brown, T. C., Fellows, C. M., Naidu, R., & Komarneni, S. (2021). Highly efficient removal of antimonite (Sb (III)) from aqueous solutions by organoclay and organozeolite: Kinetics and Isotherms. *Applied Clay Science, 203*, 106004.

Bertuoli, P. T., Piazza, D., Scienza, L. C., & Zattera, A. J. (2014). Preparation and characterization of montmorillonite modified with 3-aminopropyltriethoxysilane. *Applied Clay Science, 87*, 46–51.

Bhattacharyya, R., & Ray, S. K. (2015). Removal of congo red and methyl violet from water using nano clay filled composite hydrogels of poly acrylic acid and polyethylene glycol. *Chemical Engineering Journal, 260*, 269–283.

Bolto, B., Dixon, D., & Eldridge, R. (2004). Ion exchange for the removal of natural organic matter. *Reactive and Functional Polymers, 60*, 171–182.

Chen, H., Koopal, L. K., Xiong, J., Avena, M., & Tan, W. (2017). Mechanisms of soil humic acid adsorption onto montmorillonite and kaolinite. *Journal of Colloid and Interface Science, 504*, 457–467.

Chen, H., Li, Q., Wang, M., Ji, D., & Tan, W. (2020). XPS and two-dimensional FTIR correlation analysis on the binding characteristics of humic acid onto kaolinite surface. *Science of the Total Environment, 724*, 138154.

Collado, S., Oulego, P., Suarez-Iglesias, O., & Diaz, M. (2018). Biodegradation of dissolved humic substances by fungi. *Applied Microbiology and Biotechnology, 102*, 3497–3511.

Dehghani, M. H., Zarei, A., Mesdaghinia, A., Nabizadeh, R., Alimohammadi, M., Afsharnia, M., & McKay, G. (2018). Production and application of a treated bentonite–chitosan composite for the efficient removal of humic acid from aqueous solution. *Chemical Engineering Research and Design, 140*, 102–115.

Deng, S., & Bai, R. (2003a). Aminated polyacrylonitrile fibers for humic acid adsorption: behaviors and mechanisms. *Environmental Science & Technology, 37*, 5799–5805.

Deng, S., & Bai, R. (2004). Adsorption and desorption of humic acid on aminated polyacrylonitrile fibers. *Journal of Colloid and Interface Science, 280*, 36–43.

Deng, S., & Bai, R. B. (2003b). Aminated Polyacrylonitrile Fibers for Humic Acid Adsorption: Behaviors and Mechanisms. *Environmental Science & Technology, 37*, 5799–5805.

Doulia, D., Leodopoulos, C., Gimouhopoulos, K., & Rigas, F. (2009). Adsorption of humic acid on acid-activated Greek bentonite. *Journal of Colloid and Interface Science, 340*, 131–141.

Feng, Y., Hasegawa, Y., Suga, T., Nishide, H., Yang, L., Chen, G., & Li, S. (2019). Tuning conformational H-bonding arrays in aromatic/alicyclic polythiourea toward high energy-storable dielectric material. *Macromolecules, 52*, 8781–8787.

Freundlich, H. (1907). Über die adsorption in lösungen. *Zeitschrift für Physikalische Chemie, 57*, 385–470.

Ge, X., Zhang, Z., Yu, H., Zhang, B., & Cho, U. R. (2018). Study on viscoelastic behaviors of bentonite/nitrile butadiene rubber nanocomposites compatibilized by

https://doi.org/10.1007/s42860-023-00233-9 Published online by Cambridge University Press

different silane coupling agents. *Applied Clay Science, 157*, 274–282.

Glatstein, D. A., & Francisca, F. M. (2015). Influence of pH and ionic strength on Cd, Cu and Pb removal from water by adsorption in Na-bentonite. *Applied Clay Science, 118*, 61–67.

Gupta, V. K., Gupta, M., & Sharma, S. (2001). Process development for the removal of lead and chromium from aqueous solutions using red mud-an aluminium industry waste. *Water Research, 35*, 1125–1134.

He, H., Duchet, J., Galy, J., & Gerard, J.-F. (2005). Grafting of swelling clay materials with 3-aminopropyltriethoxysilane. *Journal of Colloid and Interface Science, 288*, 171–176.

Ho, Y. S., & McKay, G. (1998). A comparison of chemisorption kinetic models applied to pollutant removal on various sorbents. *Process Safety and Environmental Protection, 76*, 332–340.

Ho, Y. S., & McKay, G. (1999). Pseudo-second order model for sorption processes. *Process biochemistry, 34*, 451–465.

Hua, J. M. (2018). Adsorption of low-concentration arsenic from water by co-modified bentonite with manganese oxides and poly(dimethyldiallylammonium chloride). *Journal of Environmental Chemical Engineering, 6*, 156–168.

Huskic, M., Zigon, M., & Ivankovic, M. (2013). Comparison of the properties of clay polymer nanocomposites prepared by montmorillonite modified by silane and by quaternary ammonium salts. *Applied Clay Science, 85*, 109–115.

Jarvis, K. L., & Majewski, P. (2012). Plasma polymerized allylamine coated quartz particles for humic acid removal. *Journal of Colloid and Interface Science, 380*, 150–158.

Lan, T., Wu, P., Liu, Z., Stroet, M., Liao, J., Chai, Z., Mark, A. E., Liu, N., & Wang, D. (2022). Understanding the Effect of pH on the Solubility and Aggregation Extent of Humic Acid in Solution by Combining Simulation and the Experiment. *Environmental Science & Technology, 56*, 917–927.

Langmuir, I. (1916). The Constitution and Fundamental Properties of Solids and Liquids. Part I. Solids. *Journal of the American Chemical Society, 38*, 2221–2295.

Langmuir, I. (1918). The adsorption of gases on plane surfaces of glass, mica and platinum. *Journal of the American Chemical Society, 40*, 1361–1403.

Li, S. X., He, M. X., Li, Z. J., Li, D. M., & Pan, Z. B. (2017). Removal of humic acid from aqueous solution by magnetic multi-walled carbon nanotubes decorated with calcium. *Journal of Molecular Liquids, 230*, 520–528.

Lowe, J., & Hossain, M. M. (2008). Application of ultrafiltration membranes for removal of humic acid from drinking water. *Desalination, 218*, 343–354.

Majzik, A., & Tombacz, E. (2007). Interaction between humic acid and montmorillonite in the presence of calcium ions I. Interfacial and aqueous phase equilibria: Adsorption and complexation. *Organic Geochemistry, 38*, 1319–1329.

Mekidiche, M., Khaldi, K., Nacer, A., Boudjema, S., Ameur, N., Lerari-Zinai, D., Bachari, K., & Choukchou-Braham, A. (2021). Organometallic modified montmorillonite application in the wastewater purification: Pollutant photodegradation and antibacterial efficiencies. *Applied Surface Science, 569*, 151097.

Mo, W., He, Q., Su, X., Ma, S., Feng, J., & He, Z. (2018). Preparation and characterization of a granular bentonite composite adsorbent and its application for Pb^{2+} adsorption. *Applied Clay Science, 159*, 68–73.

Naderi, A., Delavar, M. A., Ghorbani, Y., Kaboudin, B., & Hosseini, M. (2018). Modification of nano-clays with ionic liquids for the removal of Cd (II) ion from aqueous phase. *Applied Clay Science, 158*, 236–245.

Peng, X., Luan, Z., Chen, F., Tian, B., & Jia, Z. (2005). Adsorption of humic acid onto pillared bentonite. *Desalination, 174*, 135–143.

Quan, X., Sun, Z., Xu, J., Liu, S., Han, Y., Xu, Y., Meng, H., Wu, J., & Zhang, X. (2020). Construction of an aminated MIL-53(Al)-functionalized carbon nanotube for the efficient removal of bisphenol AF and metribuzin. *Inorganic Chemistry, 59*, 2667–2679.

Saldaña-Robles, A., Saldaña-Robles, N., Saldaña-Robles, A. L., Damian-Ascencio, C., Rangel-Hernández, V. H., & Guerra-Sanchez, R. (2017). Arsenic removal from aqueous solutions and the impact of humic and fulvic acids. *Journal of Cleaner Production, 159*, 425–431.

Salman, M., El-Eswed, B., & Khalili, F. (2007). Adsorption of humic acid on bentonite. *Applied Clay Science, 38*, 51–56.

Shaker, A. M., Komy, Z. R., Heggy, S. E. M., & El-Sayed, M. E. A. (2012). Kinetic Study for Adsorption Humic Acid on Soil Minerals. *Journal of Physical Chemistry A, 116*, 10889–10896.

Sposito, G. (1979). Derivation of the Langmuir equation for ion exchange reactions in soils. *Soil Science Society of America Journal, 43*, 197–198.

Sudoh, R., Islam, M. S., Sazawa, K., Okazaki, T., Hata, N., Taguchi, S., & Kuramitz, H. (2015). Removal of dissolved humic acid from water by coagulation method using polyaluminum chloride (PAC) with calcium carbonate as neutralizer and coagulant aid. *Journal of Environmental Chemical Engineering, 3*, 770–774.

Tan, X., Zhou, X., Hua, R. & Zhang, Y. Technologies for the removal of humic acid from water: A short review of recent developments. , 2010, IEEE, 1-5.

Tao, Q., Xu, Z., Wang, J., Liu, F., Wan, H., & Zheng, S. (2010). Adsorption of humic acid to aminopropyl functionalized SBA-15. *Microporous and Mesoporous Materials, 131*, 177–185.

Wang, J., Li, H., & Yue, D. (2022). Enhanced adsorption of humic/fulvic acids onto urea-derived graphitic carbon nitride. *Journal of Hazardous Materials, 424*, 127643.

Wang, J., Liu, S., & Tang, W. (2017). Enhanced adsorption of humic acid on APTES modified palygorskite: behavior and mechanism. *Desalination and Water Treatment, 79*, 313–321.

Wang, J., Yue, D., Cui, D., Zhang, L., & Dong, X. (2021a). Insights into adsorption of humic substances on graphitic carbon nitride. *Environmental Science & Technology, 55*, 7910–7919.

Wang, L., Dionysiou, D. D., Lin, J., Huang, Y., & Xie, X. (2021b). Removal of humic acid and Cr(VI) from water using ZnO–30N-zeolite. *Chemosphere, 279*, 130491.

Wang, R. X., Wen, T., Wu, X. L., & Xu, A. W. (2014). Highly efficient removal of humic acid from aqueous solutions by Mg/Al layered double hydroxides-Fe_3O_4 nanocomposites. *RSC Advances, 4*, 21802–21809.

https://doi.org/10.1007/s42860-023-00233-9 Published online by Cambridge University Press

Xie, L., Lu, Q., Mao, X., Wang, J., Han, L., Hu, J., Lu, Q., Wang, Y., & Zeng, H. (2020). Probing the intermolecular interaction mechanisms between humic acid and different substrates with implications for its adsorption and removal in water treatment. *Water Research, 176*, 115766.

Yan, L., Low, P., & Roth, C. (1996a). Swelling pressure of montmorillonite layers versus H-O-H bending frequency of the interlayer water. *Clays and Clay Minerals, 44*, 749–756.

Yan, L., Low, P. F., & Roth, C. B. (1996b). Enthalpy changes accompanying the collapse of montmorillonite layers and the penetration of electrolyte into interlayer space. *Journal of Colloid and Interface Science, 182*, 417–424.

Yan, L., Roth, C. B., & Low, P. F. (1996c). Changes in the Si−O vibrations of smectite layers accompanying the sorption of interlayer water. *Langmuir, 12*, 4421–4429.

Yan, L., Roth, C. B., & Low, P. F. (1996d). Effects of monovalent, exchangeable cations and electrolytes on the infrared vibrations of smectite layers and interlayer water. *Journal of Colloid and Interface Science, 184*, 663–670.

Yan, L., & Stucki, J. W. (1999). Effects of Structural Fe Oxidation State on the Coupling of Interlayer Water and Structural Si−O Stretching Vibrations in Montmorillonite. *Langmuir, 15*, 4648–4657.

Yan, L., & Stucki, J. W. (2000). Structural perturbations in the solid–water interface of redox transformed nontronite. *Journal of Colloid and Interface Science, 225*, 429–439.

Yang, H., Luo, B., Lei, S., Wang, Y., Sun, J., Zhou, Z., Zhang, Y., & Xia, S. (2021). Enhanced humic acid degradation by Fe_3O_4/ultrasound-activated peroxymonosulfate : Synergy index, non-radical effect and mechanism. *Separation and Purification Technology, 264*, 118466.

Zhang, J., Lu, W., Zhan, S., Qiu, J., Wang, X., Wu, Z., Li, H., Qiu, Z., & Peng, H. (2021). Adsorption and mechanistic study for humic acid removal by magnetic biochar derived from forestry wastes functionalized with Mg/Al-LDH. *Separation and Purification Technology, 276*, 119296.

Zhang, Y.-J., Ou, J.-L., Duan, Z.-K., Xing, Z.-J., & Wang, Y. (2015). Adsorption of Cr(VI) on bamboo bark-based activated carbon in the absence and presence of humic acid. *Colloids and Surfaces A-Physicochemical and Engineering Aspects, 481*, 108–116.

Zhang, Y. B., Lu, M. M., Su, Z. J., Wang, J., Tu, Y. K., Chen, X. J., Cao, C. T., Gu, F. Q., Liu, S., & Jiang, T. (2019). Interfacial reaction between humic acid and Ca-Montmorillonite: Application in the preparation of a novel pellet binder. *Applied Clay Science, 180,* 105177.

Zhao, L., Luo, F., Wasikiewicz, J. M., Mitomo, H., Nagasawa, N., Yagi, T., Tamada, M., & Yoshii, F. (2008). Adsorption of humic acid from aqueous solution onto irradiation-crosslinked carboxymethylchitosan. *Bioresource Technology, 99*, 1911–1917.

Zhou, T., Huang, S., Niu, D. J., Su, L. H., Zhen, G. Y., & Zhao, Y. C. (2018). Efficient Separation of Water-Soluble Humic Acid Using (3-Aminopropyl)triethoxysilane (APTES) for Carbon Resource Recovery from Wastewater. *ACS Sustainable Chemistry & Engineering, 6*, 5981–5989.

Zhou, T., Zhao, X., Wu, S., Su, L., & Zhao, Y. (2019). Efficient capture of aqueous humic acid using a functionalized stereoscopic porous activated carbon based on poly(acrylic acid)/food-waste hydrogel. *Journal of Environmental Sciences, 77*, 104–114.

Springer Nature or its licensor (e.g. a society or other partner) holds exclusive rights to this article under a publishing agreement with the author(s) or other rightsholder(s); author self-archiving of the accepted manuscript version of this article is solely governed by the terms of such publishing agreement and applicable law.

https://doi.org/10.1007/s42860-023-00233-9 Published online by Cambridge University Press